AIMS Geosciences

AIMS Geosciences, 10(3): 498–523.
DOI: 10.3934/geosci.2024026
Received: 03 April 2024
Revised: 17 June 2024
Accepted: 04 July 2024
Published: 15 July 2024

http://www.aimspress.com/journal/geosciences

Research article

Assessment of rock mass properties and load-bearing potential in low-grade metamorphic rocks: A study from the Tigray region, Ethiopia

Shishay T Kidanu[1,*], Gebremedhin Berhane[2,*], Mogos Amare[3] and Mulubrhan Kebede[4]

[1] Dept. of Civil, Geological, and Environmental Engineering; University of Alaska Fairbanks; USA
[2] School of Earth Sciences, Mekelle University, Ethiopia
[3] Tigray Water Works Study, Design and Supervision Enterprise (TWWSDSE), Ethiopia
[4] School of Mines, Aksum University, Ethiopia

* **Correspondence:** Email: stkidanu@alaska.edu; gmedhin2009@gmail.com.

Abstract: This study presents an engineering geological investigation aimed at assessing the bearing capacity of the proposed site for the Meli gold processing plant (GPP) located in the northwestern region of Tigray, Ethiopia. The geological composition of the site predominantly comprises low-grade metamorphic rocks, with intermediate metavolcanic rocks being the most prevalent. This research utilized an innovative combination of empirical methodologies, including the Hoek–Brown and Mohr–Coulomb criteria, to evaluate the strength and elasticity characteristics of the rock mass. Additionally, the rock mass foundation for the GPP was rigorously classified using renowned systems such as the rock mass rating (RMR), quality index (Q), and geological strength index (GSI). Employing five different empirical equations to estimate bearing capacity, this study significantly advances our understanding by comparing these diverse methodologies, which is a novel approach in this geological context where engineering property data are scarce or non-existent. The bearing capacities determined using the Hoek–Brown and Mohr–Coulomb criteria ranged from 11.6 to 46.2 MPa and 7.9 to 10.5 MPa, respectively. These findings not only offer valuable insights into the assessment of bearing capacity in metamorphic rock formations but also underscore the effectiveness of combining multiple empirical approaches to enhance the reliability of geological assessments. This research contributes to the advancement of construction practices and enhances project planning strategies in comparable geological environments, particularly highlighting the utility of robust empirical data in the absence of extensive drilling data. By integrating comprehensive empirical analyses, the study provides a methodological framework that significantly aids in informed decision-making for future projects located in similar geological settings.

Keywords: bearing capacity; low-grade metamorphic rock; Meli gold processing plant, rock mass classification.

1. Introduction

The determination of ultimate bearing capacity holds paramount importance in designing foundations for various engineering structures, encompassing processing plants, factories, dams, roads, and bridges, especially when reliant on extensive rock masses [1,2]. While most rock masses are deemed suitable foundation materials, exceptions like extremely soft rocks or those with extensive jointing necessitate precise calculations of ultimate bearing capacity, particularly for structures enduring heavy foundation loads, such as skyscrapers and industrial facilities [2].

The inherent characteristics of the substrate profoundly impact its structural performance, stability, and potential risks to occupants and users. Engineering properties of in situ rock are determined from laboratory tests on intact rock samples collected from drilling cores, outcrops, or from other exposures along existing cuts [3]. However, most rocks at a foundation scale are affected by discontinuities including fractures, foliation, cleavage, bedding planes of strata, and other micro- and macro-structures [3,4]. Many researchers (e.g., Kulhawy and Goodman [5]) have suggested that it is necessary to use rock mass strength parameters in the evaluation of bearing capacity. In many cases, rock mass properties are 50%–70% of intrinsic material (measured in the laboratory) rock properties. Incorporating the influence of such discontinuities on the engineering properties or bearing capacity is possible via rock mass classification. Presently, rock mass rating (RMR) and Barton's Q value are preferred for determining rock mass classification and rock mass properties [3–6]. Hence, a thorough site investigation is imperative to collect relevant rock mass parameters and to design foundations that are both safe and economically viable. Consequently, this study undertook an engineering geological assessment to analyze the geo-materials at the site, ascertain the optimal foundation depth, and evaluate the bearing capacity of the underlying geo-material.

The characterization of the rock mass at this site, including parameters like the geological strength index (GSI), uniaxial compression strength, and in situ deformation modulus of the intermediate metavolcanic (IMV) unit, was derived from comprehensive field and laboratory analyses. The aim of this research was to provide crucial insights into the assessment of bearing capacity in metamorphic rock, thereby guiding future projects in analogous geological contexts. This research contributes to advancing construction practices and enhancing project planning strategies in comparable geological environments.

2. Description of the study site

2.1. Location

This study was conducted at a proposed site for the Meli gold processing plant (GPP), located approximately 72 km southwest of Shire-Endaslassie, the administrative center of the Northwestern Zone of the Tigray Regional State in Northern Ethiopia.

The site's geographic coordinates fall within UTM Zone 37, with the easting ranging from 0396250 to 0396450 m East and the northing from 1543450 to 1543650 m North. Figure 1 provides a streamlined map illustrating the location of the study area.

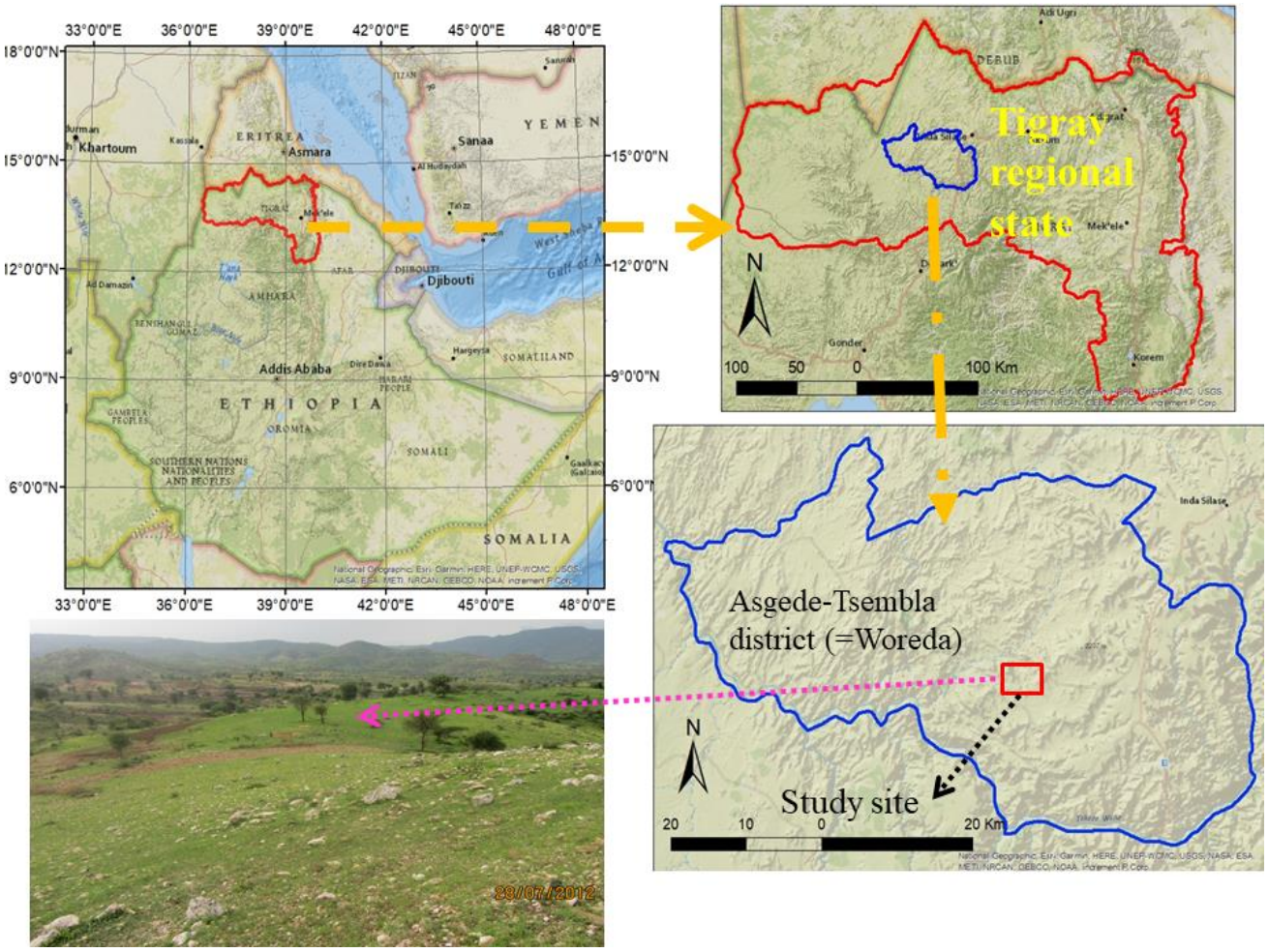

Figure 1. Simplified location map of Meli gold project area and field photograph showing of the site.

2.2. Geological background

In earlier studies, the Precambrian geology of Northern Ethiopia was classified into two main lithologic groups: the Tsaliet and Tembien [7,8]. Subsequent research indicated that the Precambrian geology of this region is part of the Arabian-Nubian Shield (ANS) [9]. The concept of ophiolite belts in the basement of North-East Africa was introduced based on ophiolite sutures and associated shear zones, which led to the division of the Red Sea Hills of Sudan or the Nubian Shield into five terranes. Geological investigations in northern Eritrea [10] revealed that the Precambrian geology of the area consists of four accreted terranes: Barka, Hagar, Adobha Abiy, and Nakfa, from west to east.

A lithostructural mapping has been conducted in the northwestern part of Tigray, specifically the Axum sheet, supported by petrochemistry [11,12]. By integrating major and trace element data with field geological and structural studies, they identified east-to-west accreted intra-oceanic arc

sequences with diverse lithological and geochemical characteristics. This supports the arc accretion model proposed for the crustal growth of the ANS [12].

Geological, geochemical, and geochronological data from the Axum map sheet [6–8] further revealed that the Precambrian geology of northern Ethiopia consists of five petrogenetically distinct tectonostratigraphic blocks: Shiraro, Adi Hageray, Adi Nebrid, Chila, and Adwa blocks.

The geochemistry of metavolcanic rocks in this region varies, ranging from mid-oceanic ridge basalts (MORB) in the Adi Hageray block, to mixed MORB-IAT (island arc tholeiitic) chemistry in the Zager mafic-ultramafic belt, to immature island-arc tholeiitic (IIAT) in the Adi Nebrid block [12]. East of the Adi Nebrid block, the Chila block is characterized by a sequence of fine-grained phyllite and chert, often carbonaceous, with minor occurrences of marble and greywackes.

The Adi-Nebrid block, which represents the northeastern extension of the Rahwa area, consists of a thick sequence of felsic to basic metavolcanic rocks, pyroclastic rocks, and associated immature volcaniclastic sediments [11–13].

3. Methodology

To ensure a thorough assessment, the study adopted the following comprehensive methodology:

Discontinuity survey: In alignment with the recommendations of the International Society for Rock Mechanics [14], a detailed discontinuity survey was carried out. This process involved the acquisition of 203 data points concerning orientation, aperture, infilling, and spacing within the intermediate and basic metavolcanic units. In addition to these measurements, 11 disturbed soil samples and 3 intact rock samples were gathered for subsequent laboratory analyses. This phase also included a review of preexisting geotechnical log data pertinent to the area surrounding the proposed foundation site (Table 1).

Laboratory analysis: Adhering to the protocols established by the American Society for Testing and Materials (ASTM) and the ISRM [14,15], a series of laboratory analyses were conducted. For the residual soils, this encompassed grain size analysis, Atterberg limits determination, and the measurement of natural moisture content. The analysis of rock samples included water absorption tests, point load tests, and the estimation of unconfined compressive strength, offering a comprehensive view of the material properties.

Discontinuity orientation and analysis: The evaluation of discontinuity orientations was facilitated by the application of Rockworks15 software [16], which utilizes equal-area stereographic projection for data processing. The outcomes of this analysis were illustrated through rose diagrams and statistical distributions (bar graphs), providing a clear visual representation of the discontinuity orientations within the study area.

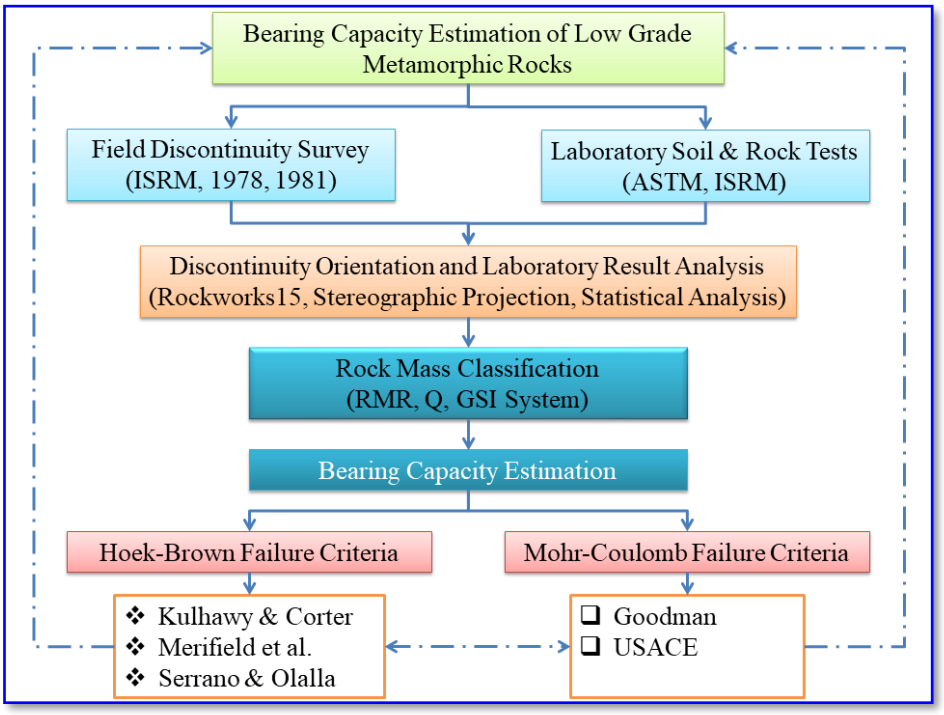

Figure 2. Flowchart showing the overall methodological approach of the study.

Rock mass characterization and classification: The rock mass was subjected to an extensive characterization and classification process, employing the geomechanics classification system [17] and the tunnelling quality index (Q) classification methodology [18]. This step involved a meticulous evaluation of various parameters to ascertain the quality of the rock mass.

Rock strength and weathering evaluation: The assessment of rock strength incorporated both field and laboratory methods. Field strength was estimated using geological hammer techniques, adhering to the guidelines proposed by [19] and the International Society for Rock Mechanics [14]. Laboratory evaluations involved point load tests, which provide a quantifiable measure of rock strength. The classification of rock weathering degrees was conducted in accordance with the system developed by [20], offering a comprehensive understanding of the geological weathering processes affecting the site.

Bearing capacity estimation: To ascertain the bearing capacity of the site's rock, a multifaceted approach was employed, leveraging several established methodologies. These methods encompassed the analytical frameworks proposed by Kulhawy and Carter [21], Goodman [22], Merifield et al. [2], Serrano and Olalla [23], and the United States Army Corps of Engineers [24]. Each method provided a distinct perspective on bearing capacity, facilitating a robust and nuanced analysis. As pointed out in [22], no universal formula for bearing capacity of rock can be given. Several simple approaches can be utilized. The methods are from both Mohr–Coulomb and Hoek–Brown's empirical failure criteria (Figure 2).

Through the application of these methodologies, the research aimed to achieve a thorough understanding of the engineering geological characteristics and rock mass quality at the site. This comprehensive analysis underpins the estimation of bearing capacity, contributing to the body of knowledge on construction practices in similar geological settings.

Table 1. Summary of soil and rock samples collected for index tests.

№	Test pit	Depth (m)	Sample number	UTM coordinates (zone 37N)		
				East (m E)	North (m N)	Elevation (m)
1	TP-01	1.40–2.80	01	0396386	1543628	1214
2	TP-02	0.20–1.20	02	0396386	1543600	1207
3	TP-03	0.20–2.00	03	0396363	1543594	1209
4	TP-04	0.40–2.00	04	0396361	1543569	1204
5	TP-05	0.20–2.30	05	0396375	1543555	1202
6	TP-06	0.40–1.60	06	0396394	1543531	1207
7	TP-07		No sample	0396352	1543549	1201
8	TP-08	0.40–2.40	08	0396361	1543528	1209
9	TP-09	0.30–2.00	09	0396369	1543515	1207
10	TP-10	0.40–2.00	10	0396347	1543509	1210
11	TP-11	0.40–2.00	11	0396335	1543524	1208
12	TP-12	0.30–2.00	12	0396308	1543484	1210
13	TP-13		No sample	0396294	1543495	1204
14	Three intact rock samples (2 from IMV and 1 from BMV) for water absorption, density, and point load (strength) tests					

4. Results

4.1. Site geology

The detailed geological mapping of the area was initially carried out by Ezana Mining Development PLC [25]. Additionally, a comprehensive engineering geological study focusing on mining was conducted in [26]. The present study, however, was explicitly oriented toward the proposed GPP site, with a primary focus on assessing the bearing capacity. Based on these works and additional observations, the Meli gold project area was found to comprise the following geological units:

4.1.1. Intermediate metavolcanic unit (IMV)

This unit is characterized by its light to dark greenish-grey color, fine to medium grain, and moderate foliation (Figure 3a). It primarily consists of biotite, chlorite, quartz, and some actinolite and plagioclase minerals. The unit covers a significant portion of the GPP site and is in contact with the basic metavolcanic unit in the southern part and quartz porphyry/vein in the northern extreme part of the site. The foliation direction is predominantly E–W, with a southward dip. Notable foliation measurements include (080°/80° S, 080°/75° S, 090°/80° S, 275°/75° S, 080°/70° S).

4.1.2. Basic metavolcanic unit (BMV)

The basic metavolcanic unit is characterized by its dark green color, fine to medium grain, and weakly foliated to massive structure (Figure 3b). It exhibits a deep reddish to dark grey weathering color and primarily comprises amphibole minerals such as actinolite and tremolite, biotite, chlorite,

plagioclase, and quartz. The thickness of this unit varies from a few meters up to 400 meters. It is in contact with the sub-intrusive unit in its northern, eastern, and western parts and with the IMV unit and gossan in its southern parts. Notably, the BMV unit does not extensively outcrop within the proposed gold processing plant site, except on its southern side.

4.1.3. Sericite schist (QSS)

This unit is characterized by its light grey color, fine-grained, and highly deformed structure (Figure 3c). It is exposed in the southern part of the eastern Meli and the central and northern parts of the central and western Meli, respectively. The quartz sericite schist is highly sericitized and sulfidized in most parts. It covers a limited area within the site and exhibits less deformation compared with the schist in the main Meli exploration area. Additionally, it was challenging to trace its continuity from the outcrop in the eastern site toward the western direction.

Figure 3. (A) IMV unit, (B) BMV unit, and (C) QSS unit (photo taken approximately from east to west direction).

4.1.4. Quartz vein (QV)

Intense quartz veins are observed in the eastern, central, and western parts of the area, invading the metamorphic units (Figure 4). The veins range in width from a few centimeters to 20 meters and occur discontinuously along the strike. Most of the quartz veins are white and glassy, with some being sugary to milky type. Notably, a patchy outcrop is observed in the northern extreme part of the proposed gold processing plant site, with no defined orientation or estimated thickness.

These detailed geological descriptions provide valuable insights into the composition and characteristics of the geological units within the Meli gold project area, essential for the comprehensive understanding of the site's geological profile.

4.1.5. Geological structures

The study area and its surroundings exhibit various geological structures, including folds, faults, foliation, joints, and shear zones. Within the proposed GPP site, foliation, joints, and shearing have been observed. Foliation and joints are prevalent throughout the site, while the shear zone is concentrated along the sericite schist (Figure 5a). The quartz sericite schist, located in the central part

of the area, is believed to be the sheared derivative of quartz porphyry. Additionally, a series of minor sinistral dextral shears have been noted in the vicinity of the site. Brecciated and boudinaged quartz veins are also common in the area (Figure 5b).

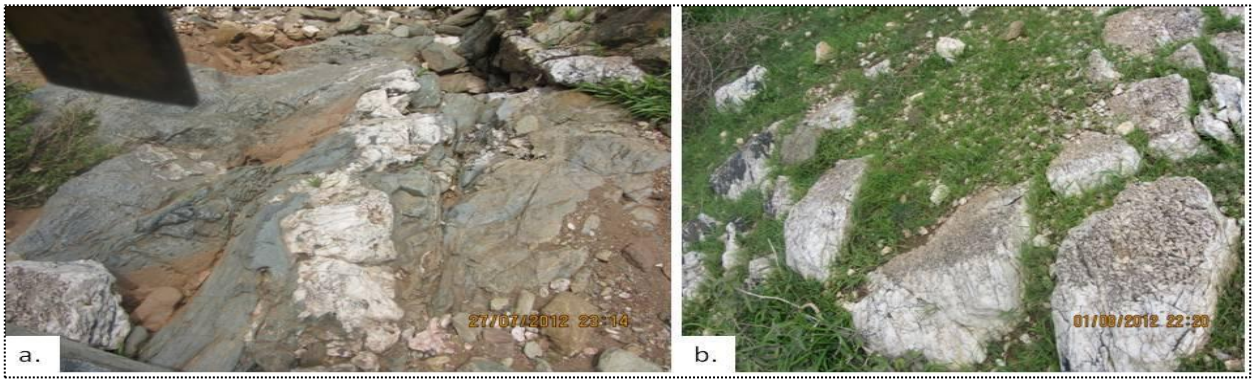

Figure 4. Quartz vein intruded at the metavolcanic rock located at the riverbed of the proposed tailing dam site, (a) west of the site and (b) at the northern end of the site.

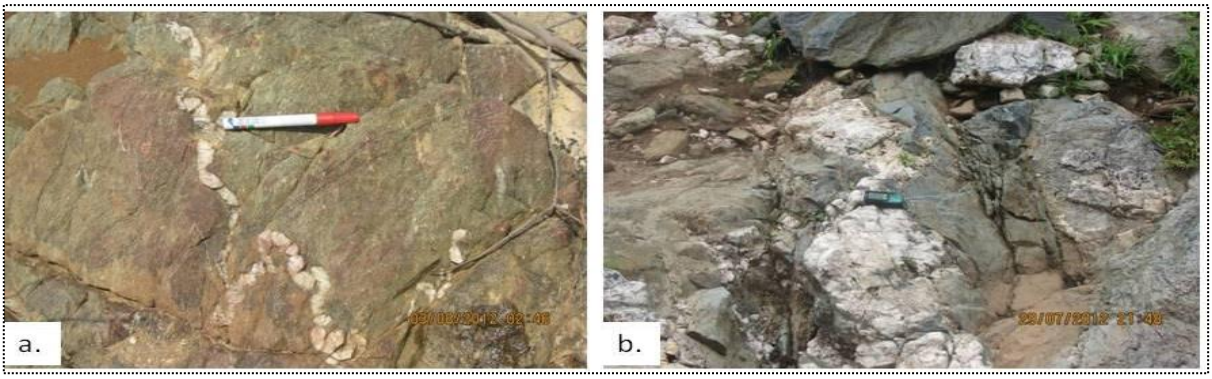

Figure 5. (a) Folded quartz veins and (b) boudinaged quartz veins.

Foliation is a prominent structure in the area, with most of the metamorphic units exhibiting a northeast general orientation. The Meli gold project, including the GPP site area, predominantly displays an east–west foliation ranging from 270° to 285° in strike and dipping toward the south. A simplified geological map of the GPP site is provided for reference (Figure 6).

These geological structures play a crucial role in shaping the geological profile of the study area and are essential considerations for the engineering geological assessment of the proposed GPP site.

4.2. Engineering geological characterization

Geologically, the study area is mainly constituted by metavolcanic rocks, medium to coarse-grained intermediate metavolcanic, and medium to fine-grained basic metavolcanic, with a small area of Quartz and sericite schist. The weathering of these rocks varies from fresh or slightly weathered (SW) intermediate metavolcanic to residual soil (RS).

Engineering geological characterization in the present site studies mainly includes field observations on soil and rock, index tests, classification of the residual soils, and discontinuity surveys for the rock masses.

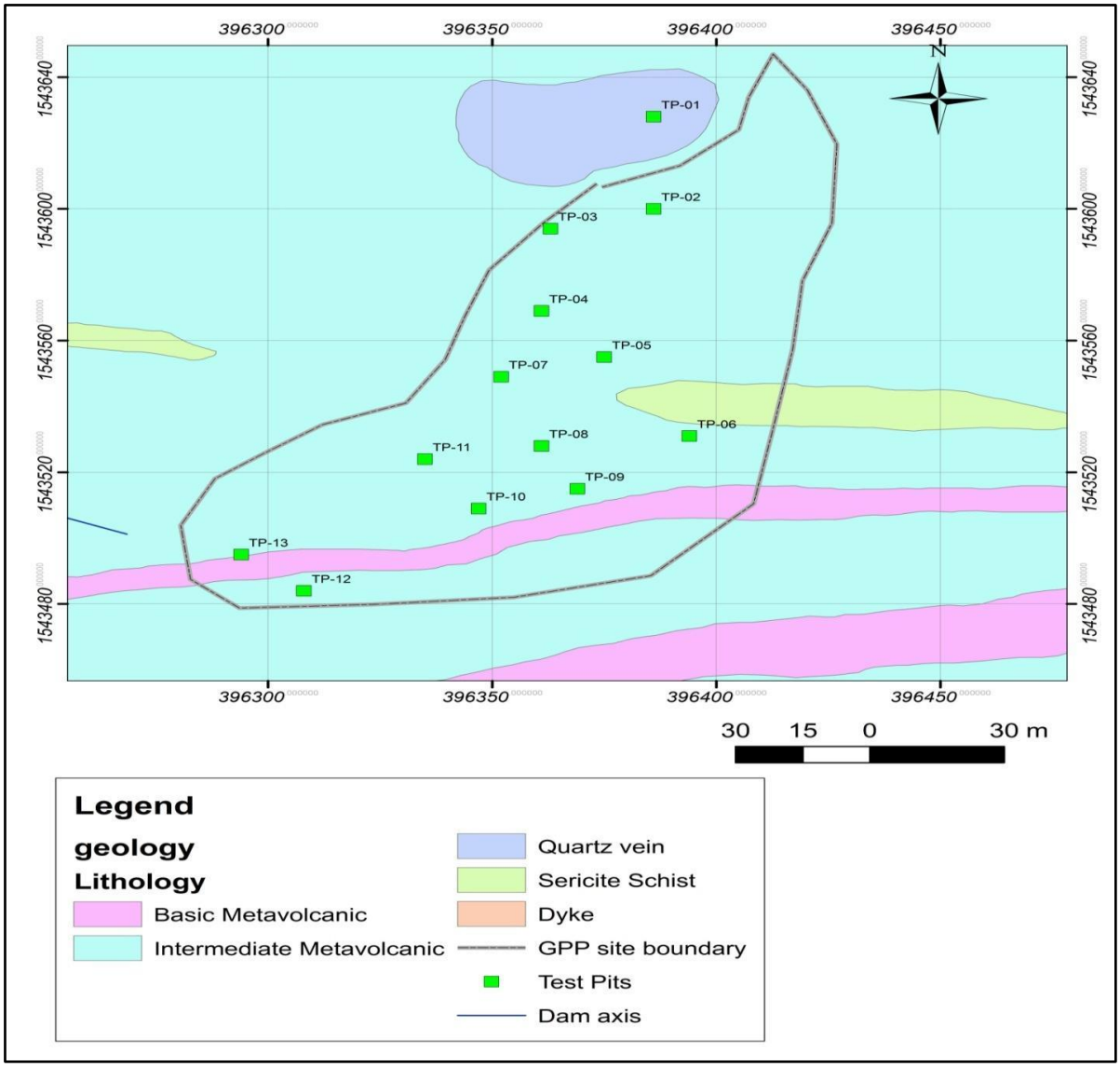

Figure 6. Simplified geological map of Meli GPP site.

4.2.1. Engineering geological layers/units

From the confirmatory excavated pit, three major and distinctive layers below the founding level of the GPP building were identified:

Layer–I (HW/RS): Highly to completely weathered rock (HW) or residual soil with an average thickness of approximately 2–3 m.

Layer–II (MW): Slightly to moderately weathered rock (MW) with a lower proportion of developed soil particles, predominantly consisting of rock fragments. The thickness of this layer is challenging to estimate using the employed investigation methods, but it is anticipated to be approximately 5–10 m thick from natural exposures.

Layer–III (FR): Slightly weathered to fresh rock (FR), which is massive and less affected by weathering processes.

Field observational data at the site and drilling data from the surrounding area revealed that the degree of weathering decreases with depth, but not uniformly. In some areas, slightly weathered rock is observed near the ground surface, while in other places within the site, this layer is encountered at greater depth. This indicates that the rock head or surface is irregular, or the mentioned layers do not have uniform thickness throughout the site.

Residual soils (completely to highly weathered metavolcanics)

The geotechnical studies concern the residual soils, ranging from completely to highly weathered metavolcanics, involved trial pitting, sampling, and laboratory testing. At the GPP, 13 trial pits, with depths ranging from 0.80 to 2.80 m, were excavated, and one disturbed sample from 11 of them (totaling 11 samples) was collected. Engineering geological logging was carried out in each test pit to determine the index properties of the soils. Groundwater-level observations were made during trial pitting and previously drilled boreholes, but no groundwater was encountered in either case. Laboratory tests included determining water content, specific gravity, grain size distribution, and Atterberg limits of soil samples obtained from the test pits.

Generally, the thickness of this layer ranged from 0.5 m at TP-07 to 2.50 m at TP-01. It exhibited almost uniform and homogenous characteristics throughout the site but varied in thickness. The soil was identified as non-plastic to low-plastic sandy silt material with a minor content of clay fraction (8%–15%). According to the Unified Soil Classification system (USCS), most of the soil samples fell under the **ML** (low plastic silt) soil group, with one exception (TP-10) classified as **CL** or **CI** (clays of low plasticity or clays of intermediate plasticity), and the other two samples were non-plastic. The laboratory index test results, including the consistency of the sandy silt and the characteristics of the soil, are summarized in Table 2.

The consistency of the sandy silt (**ML** or **CI)** was observed to be loose at shallow depths but became dense to very dense beyond 1.5 m depth. The grains of the residual soil gradually became coarser with depth, and the soil contained minor gravelly rock fragments at some locations, primarily quartz and metavolcanic rock fragments. Based on the plasticity index and the clay percentage, the soils were classified as non-plastic to moderately plastic, with low expansion potential. The soils were determined to have low plasticity, except for one soil sample that exhibited intermediate plasticity (Figure 7).

Table 2. Summary of laboratory results (index properties).

№	Test pit	Depth (m)	Specific gravity	(NMC)* (%)	Consistency limits (%)			Grain size distribution (%)			
					LL	PL	PI	Gravel	Sand	Silt	Clay
1	TP-01	1.40–2.8	2.50	10.07	33.24	28.03	5.21	0	22	70	8
2	TP-02	0.20–1.2	2.50	12.81	32.41	25.30	7.11	0	22	63	15
3	TP-03	0.20–2.0	2.55	11.90	31.79	25.96	5.83	0	32	60	8
4	TP-04	0.40–2.0	2.55	12.39	33.27	28.10	5.17	0	21	68	11
5	TP-05	0.20–2.3	2.50	10.74	33.91	26.94	6.97	0	25	64	11
6	TP-06	0.40–1.6	2.50	10.01	30.46	23.69	6.77	0	18	74	7
7	TP-08	0.40–2.4	2.55	4.56	NP	NP	NP	0	25	64	11
8	TP-09	0.30–2.0	2.55	11.86	31.03	21.73	9.30	0	29	60	11
9	TP-10	0.40–2.0	2.50	15.37	42.96	30.68	12.28	0	17	73	10
10	TP-11	0.40–2.0	2.50	14.64	33.95	27.67	6.28	0	20	66	14
11	TP-12	0.30–2.0	2.65	5.23	NP	NP	NP	0	38	54	8

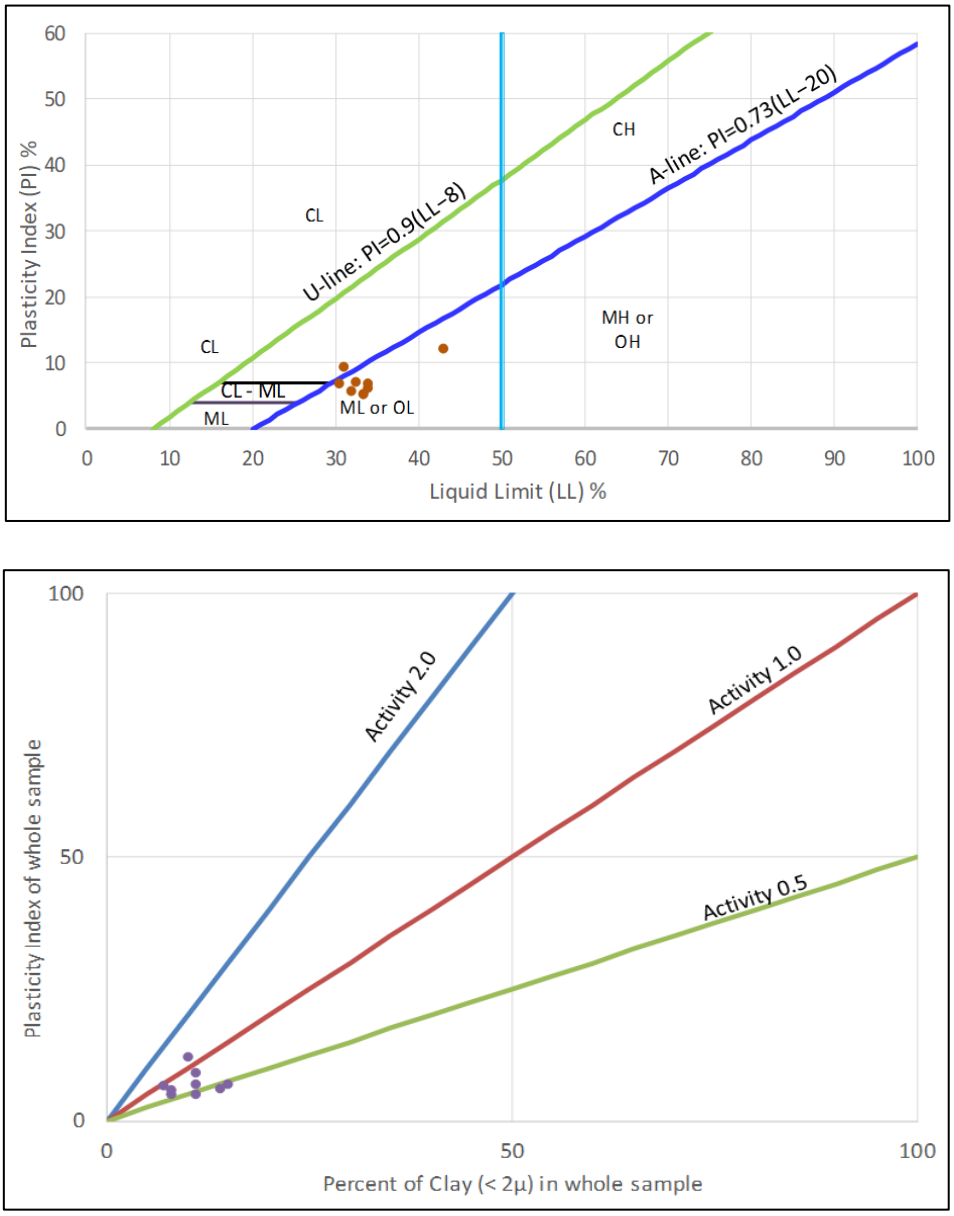

Figure 7. Plot of soil samples from the site on plasticity (top) and activity charts (bottom).

Slightly to moderately weathered metavolcanic

The slightly to moderately weathered metavolcanic unit predominates on the site below an average depth of 2 m. Outcrops of moderate to fresh rock are also observed in certain areas, mainly in the south and southwest parts of the site. The rock head (Figure 8) is expected to exhibit irregular characteristics, with shallow and deep features in some locations. This irregularity was confirmed by test pits and field surface observational data, as detailed in Table 3, where deep weathered rock (up to more than 2 m) and slightly weathered to fresh rock outcrops were observed within a very short

interval or distance at the surface. Nearly all test pit excavations were halted upon encountering refusal during manual excavation, where moderate to slightly weathered layers were encountered.

Table 3. Rock head measurements (outcrop at surface).

No.	East (m E)	North (m N)	Elevation (m)	Rock description
1	0396416	1543593	1206	IMV, HW, weak to very weak
2	0396407	1543615	1206	IMV, SW, strong
3	0396398	1543606	1212	IMV, SW, strong
4	0396370	1543602	1211	IMV, SW, strong
5	0396394	1543578	1207	IMV, SW, moderately strong
6	0396385	1543573	1207	Quartz outcrop, SW, very strong
7	0396391	1543540	1207	Sericite schist, HW, very weak
8	0396277	1543502	1205	IMV, HW, weak to very weak
9	0396298	1543503	1206	IMV, HW, weak to very weak
10	0396313	1543491	1208	IMV, SW, strong
11	0396329	1543503	1208	IMV, HW, weak to very weak
12	0396341	1543546	1203	IMV, HW, weak to very weak
13	0396357	1543558	1204	IMV, HW, weak to very weak
14	0396372	1543502	1204	IMV, HW, weak to very weak
15	0396395	1543499	1203	IMV, HW, weak to very weak
16	0396413	1543501	1199	IMV, SW, strong
17	0396423	1543513	1200	IMV, SW, strong
18	0396283	1543503	1205	IMV, SW, strong
19	0396286	1543521	1202	IMV, SW, strong
20	0396370	1543616	1214	Quartz outcrop

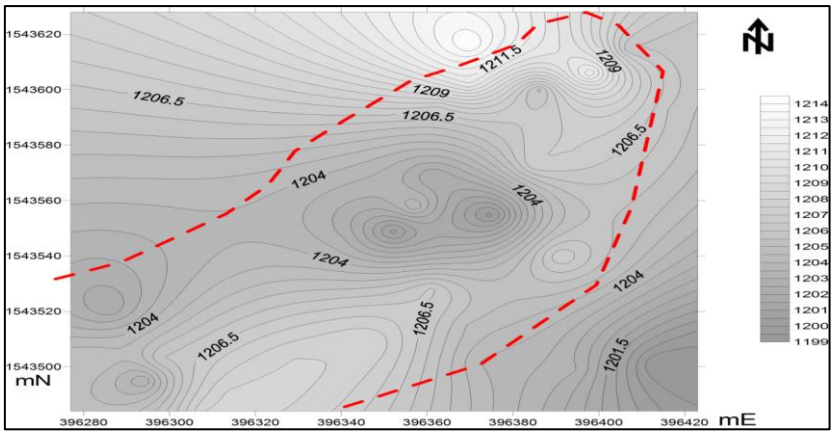

Figure 8. Approximate rock head at the GPP site (rock surface contour) using exposure and test pit data.

Given the flat to gentle terrain with a sharp increase in slope in almost all directions of the site, it is imperative for the foundation to have sufficient embedment to prevent scouring and erosion. Therefore, the bearing strata should be below 2 m (i.e., below the residual soil). Consequently, all rock mass classification and bearing capacity analysis were conducted for the slightly to moderately

weathered metavolcanic unit. From an engineering geological perspective, the IMV and BMV rocks exhibit similar engineering behavior and are considered as one unit in the rock mass classification and bearing capacity estimations. In the case of the QSS unit, insufficient discontinuity data were obtained from the field due to weathering, although it was anticipated that its engineering characteristics in its fresh condition would be similar to the other units in the area. Figure 8 provides an illustration of the rock head surface at the site.

4.2.2. Discontinuity survey

A comprehensive discontinuity survey was conducted at the site according to ISRM [9] guidelines to quantitatively describe the various aspects of the discontinuities present, including orientation, spacing, persistence, roughness, aperture, and filling. A total of 203 discontinuity data were collected from the IMV and BMV units. However, due to the unavailability of outcrops and highly weathered conditions, sufficient discontinuity measurements could not be obtained for the sericite schist and quartz exposures.

The dominant discontinuity sets identified at the site during fieldwork are categorized as E–W, NNW–SSE, and NE–SE orientations (see Figure 9). These results align with the processed data obtained. Table 4 provides a detailed quantitative description and statistical distribution of the discontinuities within the IMV unit at the site, following the ISRM [14] guidelines.

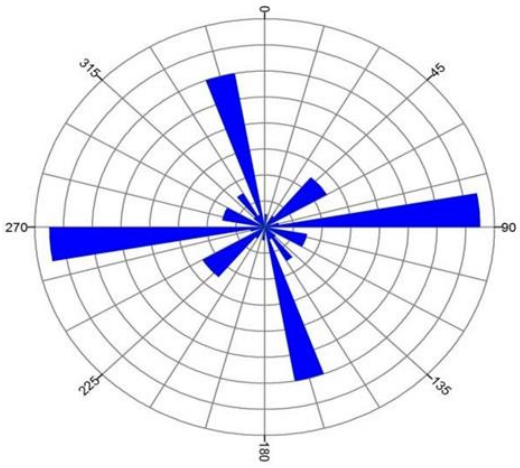

Figure 9. Rose diagram of discontinuities from the site.

Figure 10 presents histograms depicting the distribution of discontinuity spacing, aperture, persistence, roughness, and weathering degree. It is commonly observed that the majority of the discontinuities at the site are vertical, with a few dipping toward the south direction. The dominant spacing of the discontinuities falls within the range of 20–60 cm, which is classified as moderate (see Table 4).

Regarding aperture, the majority of the discontinuities exhibit sizes between 0.5 and 2.5 mm, indicating an open condition. However, there is significant variation, with a considerable number of discontinuities falling into the tight and moderately open categories as well (see Table 4 and Figure 10a). Similarly, the persistence of the discontinuities ranges from 1 to 10 m, with a higher

concentration within the 1–3 m range, indicating low persistence. The roughness conditions of the discontinuities predominantly fall into the rough and smooth undulating categories (see Figure 10b,c). The degree of weathering of the discontinuities was also quantitatively described, with highly weathered conditions prevailing at the site (see Figure 10d).

Table 4. Quantitative descriptions and statistical distributions of the discontinuities collected from the IMV unit.

	Range	Description	Frequency	Distributions (%)
Spacing (cm)	<2	Extremely close	0	0
	2–6	Very close	12	6
	6–20	Close	24	12
	20–60	Moderate	122	60
	60–200	Wide	37	18
	200–600	Very wide	8	4
	>600	Extremely wide	0	0
Aperture (mm)	<0.1	Very tight	0	0
	0.1–0.25	Tight	40	20
	0.25–0.5	Partly open	18	9
	0.5–2.5	Open	69	34
	2.5–10	Moderately open	49	24
	10–100	Very wide	27	13
	100–1000	Extremely wide	0	0
	>1000	Caverns	0	0
Roughness	I	Rough, stepped	3	1
	II	Smooth, stepped	0	0
	III	Slickensided, stepped	0	0
	IV	Rough, undulating	70	34
	V	Smooth, undulating	80	39
	VI	Slickensided, undulating	0	0
	VII	Rough, planar	48	56
	VIII	Smooth, planar	2	2
	IX	Slickensided, planar	0	0
Persistence (m)	<1	Very-low persistence	21	10
	1–3	Low persistence	93	46
	3–10	Medium persistence	89	44
	10–20	High persistence	0	0
	>20	Very-high persistence	0	0
Weathering grade	I	Fresh rock	0	0
	II	Slightly weathered (SW)	36	18
	III	Moderately weathered (MW)	62	31
	IV	Highly weathered (HW)	85	42
	V	Completely weathered (CW)	20	10
	VI	Residual soil	0	0

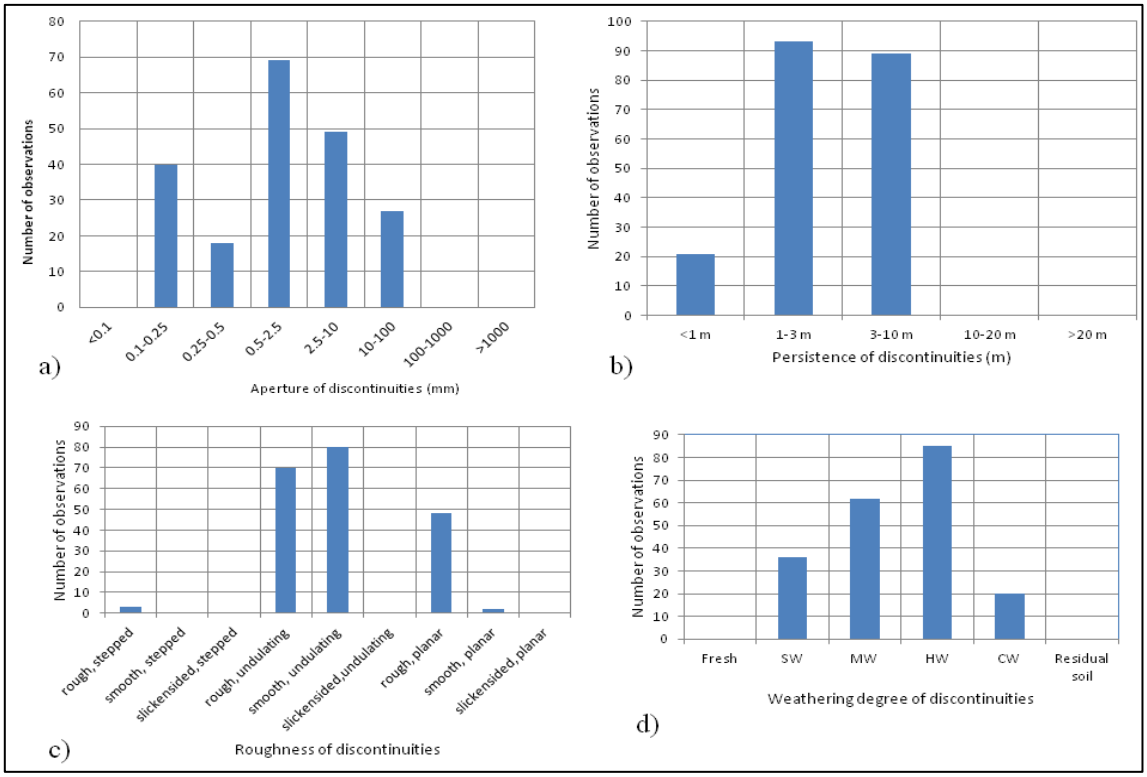

Figure 10. Statistical distributions of (a) discontinuity aperture, (b) discontinuity persistence, (c) discontinuity roughness, and (d) weathering degree of discontinuities.

4.3. Rock mass classification

Rock masses have undergone numerous tectonic and deformational activities throughout history. As a result, most rocks exhibit varying degrees of fracturing, shearing, and breaking, with features such as joints, cleavages, folds, and faults. These discontinuities play a crucial role in determining the bearing capacity of the rock mass. Their presence and characteristics significantly impact the rocks' behavior and stability, making them important considerations in engineering and construction projects. Rock mass classification systems play a crucial role in quantitatively describing the quality of rock masses. These classifications have been developed for various civil engineering projects, utilizing geological, engineering geological, and geotechnical data [27]. By providing a quantitative measure of rock masses, these classification systems help minimize subjective biases and assumptions.

Table 5. Laboratory test results for intact rock.

Sample No.	Rock type	Water absorption (%)	Density (kg/m^3)	Point load (MPa)	Intact uniaxial compressive strength UCS = 24 (I_{50}), MPa
01	IMV	0.9	2790	2.75	66
02	IMV	0.88	3015	5.52	132.48
03	BMV	1.12	2458	2.56	61.44

The most widely used rock mass classification systems worldwide include the rock mass rating (RMR) [17], the geological strength index (GSI) [28], and the Q-system [29]. At the Meli GPP site,

these classification systems were applied to the rock masses. The collected data were processed in accordance with the specific criteria of each classification system (see Tables 4 and 5). The resulting RMR and Q values were then used to estimate the properties of the rock mass and its bearing capacity (see Tables 6 and 7).

The geological strength index (GSI) was developed by [28] and is based on the visual appearance and structural characteristics of the rock mass. [30] further enhanced the GSI by incorporating additional geological properties into the Hoek–Brown failure criterion, specifically for heterogeneous weak rock masses. Alternatively, the 1989 version of the rock mass rating (RMR) and Q classification systems can be utilized to determine the GSI, as proposed by [28] using equations 1 and 2.

$$GSI = RMR - 5 \quad (1)$$

$$GSI = 9logeQ + 44 \quad (2)$$

where RMR89 is the latest version of the RMR classification system and Q′ is a modified Q given by: Q′ = (RQDxJr)/(JnxJa). The definition and meaning of the variables in the equations are indicated in Tables 6 and 7.

Table 6. RMR89 rating for IMV unit.

Classification parameters	Value of parameters	Rating
Uniaxial compressive Strength (MPa)	2.75 (point load)	7
RQD (%)	20	3
Discontinuity spacing (cm)	12.82	10
Discontinuity condition		
Persistence (m)	3–10 (Table 4)	2
Aperture (mm)	0.5–2.5	4
Roughness	Smooth to rough undulating	1 (min.) & 5 (max.)
Filling	At places quartz (>5 mm)	2
Weathering	Highly weathered (Table 4)	
Groundwater	Damp (during site investigation)	10
Basic RMR value		**39 (min.) & 43 (max.)**
Rock mass quality		**Poor to fair rock**

Table 7. Q rating for IMV unit.

Classification parameters	Value of parameters	Rating
RQD (%)	20 %	20
Joint set number (Jn)	Three joint sets plus random joints	12
Joint roughness number (Jr)	Smooth undulating	2
Joint alteration number (Ja)	Slightly altered joint walls	2
Joint water reduction factor (Jw)	Dry or minor flow	1
Stress reduction factor (SRF)	Low stress, near surface, open joints	2.5
Q		**0.668**
Rock mass quality		**Very poor rock**

The intermediate metavolcanic rock mass had an RMR value of 39, with Q values of 0.668 and Q' values of 1.667. By applying equations (1) and (2), the average GSI value was determined to be 41. A similar GSI value was also obtained using the GSI chart proposed by [19]. The Hoek–Brown [19] and Mohr–Coulomb failure criteria were employed to determine the rock mass properties of the intermediate metavolcanic (IMV). The generalized Hoek–Brown criterion, expressed in equation (3), was utilized in this analysis.

$$\sigma_1 = \sigma_3 + \sigma_{ci}\left(m_b \frac{\sigma_3}{\sigma_{ci}} + s\right)^a \quad (3)$$

where σ_1 is effective major principal stress, σ_3 is effective minor principal stress, and σ_{ci} is uniaxial compression strength of intact rock; m_b is a reduced value of the material constant m_i, and s and a are constants for the rock mass given by the relationships in equations 4, 5, and 6 [31].

$$m_b = m_i\, exp\left(\frac{GSI-100}{28-14D}\right) \quad (4)$$

$$s = \exp\left(\frac{GSI-100}{9-3D}\right) \quad (5)$$

$$a = \frac{1}{2} + \frac{1}{6}\left(e^{-GSI/15} - e^{-20/3}\right) \quad (6)$$

where D is a factor that depends upon the degree of disturbance to which the rock mass has been subjected by blast damage and stress relaxation and m_i is a material constant. In this study, the value of D was considered as zero. The calculated GSI and the Hoek–Brown constants are presented in Table 8. The uniaxial compressive strength was obtained by setting $\sigma_3 = 0$ in equation 3 and is simplified into equation 7.

$$\sigma_{cmass} = \sigma_{ci} s^a \quad (7)$$

The rock mass modulus of deformation is given by:

$$E_m(GPa) = \left(1 - \frac{D}{2}\right)\sqrt{\frac{\sigma_{ci}}{100}} \cdot 10^{\left(\frac{(GSI-10)}{40}\right)} \quad (8)$$

Equation 8 is applicable for $\sigma_{ci} \leq 100$ MPa; for $\sigma_{ci} > 100$ MPa, equation 9 is used.

$$E_m\,(GPa) = \left(1 - \frac{D}{2}\right) \cdot 10^{\left(\frac{(GSI-10)}{40}\right)} \quad (9)$$

Results of unconfined compressive strength of the rock mass and rock mass modulus of deformation based on the above equations are presented in Table 8. In addition, a computer program called RocLab by Rcoscience [32] was used to estimate the rock mass properties (see Figure 11).

4.4. Bearing capacity estimation

In general, rocks fail or rupture when the stresses acting on them exceed their tensile, compressive, or shear strengths, whichever is reached first. When it comes to designing foundations and other engineering structures, it is important to consider the properties of the rock mass rather than just the intact rock properties. This is particularly true for jointed rock masses, as these

formations are generally heterogeneous and anisotropic. They contain cracks, fissures, and joints with varying degrees of strength and other properties along these natural planes of weakness [2].

As a result, accurately establishing the bearing capacity of foundations becomes crucial for ensuring a safe and economically feasible design. By considering the properties of the rock mass and accounting for its heterogeneity and anisotropy, engineers can make informed decisions and design foundations that can withstand the expected loads and stresses.

Table 8. Rock mass properties of IMV.

Parameters	Values	Remark
Intact uniaxial compressive strength (σ_{ci}, MPa)	66	From point load test (the lower value was considered for analysis)
Geological strength index (GSI)	41	
Hoek–Brown constant of intact rock (m_i)	7	
Disturbance factor (D)	0	
Hoek–Brown constant of rock mass (m_b)	0.581	
Hoek–Brown constant of rock mass (s)	0.0014	
Hoek–Brown constant of rock mass (a)	0.511	
Strength of rock mass (σ_{cmass}, MPa)	2.322	
Modulus of deformation of rock mass (E_m, GPa)	6.25	
Tensile strength (MPa)	−0.11	
Cohesion (c, MPa)	2.523	
Internal friction angle (ϕ, degrees)	24.97	

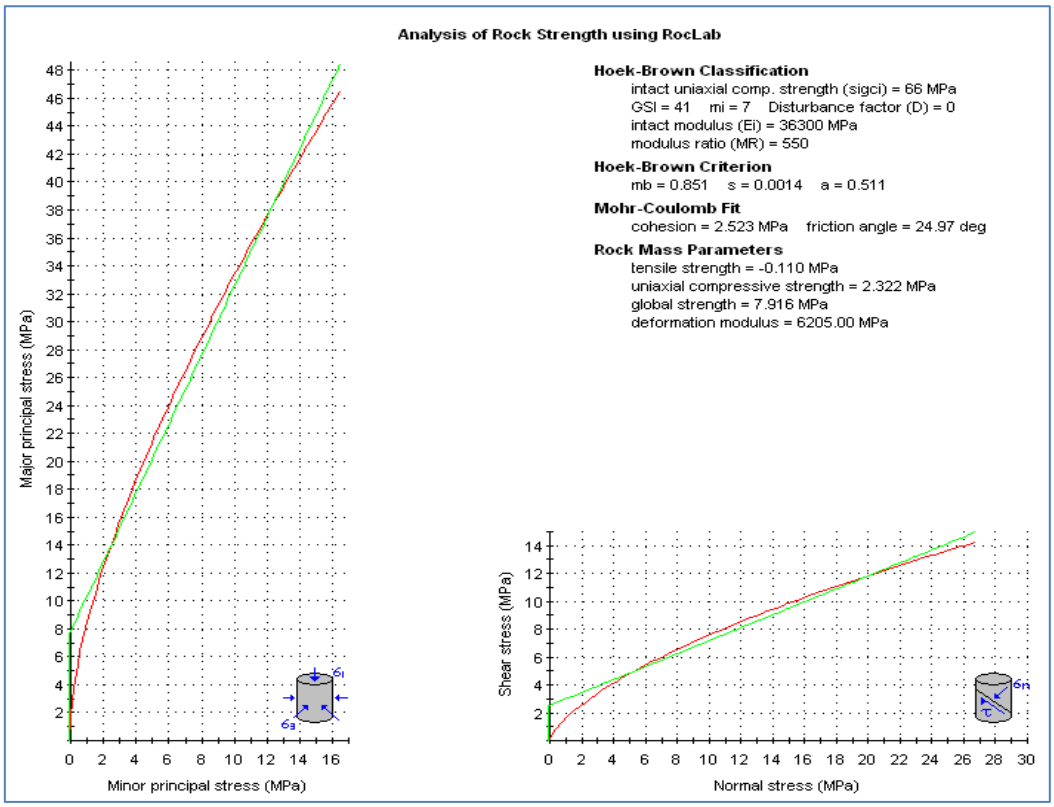

Figure 11. Analysis of rock mass strength using RocLab software [32].

When calculating the bearing capacity of a footing under load using the limit equilibrium method, it is essential to consider the complexity and variety of failure modes that can occur. These failure modes include cracking, crushing, wedging, punching, and shearing [33], as well as splitting failures. Due to the diverse nature of these failure modes, there is no universal formula that can accurately determine the bearing capacity of rocks [22].

In the present study, the bearing capacity was computed using various equations that incorporate the Hoek–Brown and Mohr–Coulomb empirical failure criteria. For instance, in [19] authors proposed the following equation (equation 10) to calculate the ultimate bearing capacity of a rock mass:

$$q_{ult} = \sigma_{ci}(s^a + (m_b s^a + s)^a) \quad (10)$$

where σ_{ci} = uniaxial compressive strength of the intact rock (MPa)

s, a = Hoek–Brown rock mass constant, and
m_b = Hoek–Brown rock material constant (reduced value of m_i).

In [22], authors proposed that the bearing capacity of a homogeneous and discontinuous rock mass should not be lower than the unconfined compressive strength of the rock mass surrounding the footing. This unconfined compressive strength can be considered as a lower bound for the bearing capacity. In cases where the rock mass has a constant angle of internal friction (ϕ) and unconfined compressive strength (σci), the bearing capacity can be estimated using equation 11.

$$q_{ult} = \sigma_{ci}(N_\phi + 1) \quad (11)$$

where $N_\phi = \left(45 + \frac{\phi}{2}\right)$

Serrano and Olalla (1994) proposed equation 12 for the evaluation of the ultimate bearing capacity of rock masses.

$$q_{ult} = \beta_n(N_\beta - \zeta_n) \quad (12)$$

where
N_β= bearing capacity factor; in this study, it was determined from m_i and the GSI approach,
β_n= strength modulus of the rock mass, and
ζ_n = rock mass toughness
β_n and ζ_n can be calculated using equations 13 and 14.

$$\beta_n = \sigma_{ci} A_n \quad (13)$$

$$\zeta_n = \frac{s}{(m_b A_n)} \quad (14)$$

where
An = function of the normalized external load calculated from equation 15.

$$A_n = \left(\frac{m_b\,(1-a)}{2^{\frac{1}{a}}}\right)^{\frac{a}{1-a}} \quad \text{..... (15)}$$

Merifield et al. [2] suggested a different equation (equation 16) for ultimate bearing capacity assessment:

$$q_{ult} = \sigma_{ci} N_\sigma \quad \text{..... (16)}$$

where

σ_{ci}= uniaxial compressive strength of the intact rock (MPa), and

N_σ= bearing capacity factor; in this study, it was determined from m_i and the GSI approach (graph).

For unconfined compression failure, USACE [24] suggested equation 17 to estimate the ultimate bearing capacity:

$$q_{ult} = 2C\ tan\ tan\ \left(45 + \frac{\phi}{2}\right) \quad \text{..... (17)}$$

where C = the cohesion intercepts for the rock mass and ϕ = angle of internal friction for the rock mass.

Table 9 provides a summary of the ultimate bearing capacities calculated using each of the equations. It is important to note that the ultimate bearing capacities obtained from different empirical equations varied. This difference in the results can be attributed to the distinct parameters considered in each equation. In particular, the use of the geological strength index (GSI) in the equations proposed by [34] and [2] tends to overestimate the bearing capacity. On the other hand, two equations based on the Mohr–Coulomb failure criteria, namely [22,24], resulted in underestimation or conservative bearing capacity values.

Table 9. Calculated ultimate bearing capacity of the rock mass (IMV unit).

Empirical equations (methods)	Ultimate bearing capacity (MPa)	Remark
Kulhawy and Carter (1992)	11.6	Hoek–Brown failure criteria
Goodman (1989)	10.5	Mohr–Columb failure criteria
Merifield et al. (2006)	46.2	Hoek–Brown failure criteria
Serrano and Olalla (1994)	26.4	Hoek–Brown failure criteria
USACE (1994)	7.9	Mohr–Columb failure criteria
Average	**20.5**	

5. Discussion

The Meli GPP was planned to be constructed on the slightly to moderately weathered intermediate metavolcanic (IMV) rock at an average depth of 2 m below the original ground surface. The characterization of the rock mass at this site, including parameters such as the geological strength index (GSI), uniaxial compression strength, and in situ deformation modulus of the IMV unit, was derived from comprehensive field and laboratory analyses. Utilizing the Q and rock mass

rating (RMR) classification systems, the IMV unit was classified within ranges indicative of very poor and poor to fair rock mass quality, respectively. The RocLab software, implementing the Hoek–Brown empirical failure criterion, calculated the rock mass strength to be 2.322 MPa.

The ultimate bearing capacity values of the IMV rock mass were obtained using empirical methods and ranged from approximately 8 to 46 MPa. According to the equations proposed by Kulhawy and Carter [21] and Goodman [22], the average ultimate bearing capacity of the rock mass was estimated to be around 11 MPa. Conversely, the equations suggested by Serrano and Olalla [34] and Merifield et al. [2] yielded an average value of 33.3 MPa, while the USACE [24] equation resulted in an estimate of approximately 8 MPa. These differences in bearing capacity results can be attributed to the various parameters considered in each equation. Notably, the inclusion of GSI in the equations proposed by Serrano and Olalla [34] and Merifield et al. [2] led to an overestimation of the bearing capacity.

It is important to note that the results of this study are specific to the Meli GPP construction project and are intended to provide general recommendations for future projects in the area. The conclusions drawn from this study suggest that using rock mass strength parameters from rock mass classification systems provides a reasonable estimation of the bearing capacity for jointed rock masses. However, additional adjustments may be necessary for the intended load distribution during the final design phase. Furthermore, field data and limited subsurface observations indicated that with increasing depth, the degree of weathering and joint aperture decreases, while joint spacing increases. Therefore, if the intended load distribution from the processing plant and associated structures exceeds the estimated bearing capacity, it may be necessary to increase the depth of the foundation to reach better bearing strata.

Considering the uncertainties inherent in natural rock masses, it is recommended to adopt lower or conservative values for bearing capacity during the design process. It is important to note that this study was conducted with limited subsurface or borehole data. Extrapolation or correlation from existing boreholes in the area was challenging, as most of them were drilled for different purposes and primarily encountered gossan material, which is essentially soil. Additionally, the variations in the degree of weathering from place to place further hindered reasonable correlations. Consequently, a significant portion of the analyses relied on limited data. For future projects in the area, it is advisable to undertake comprehensive borehole drilling at the outset, particularly for larger-sized and load-bearing structures, to enhance verification and facilitate design modifications.

During the site investigation campaign, no groundwater was encountered within the depth of interest or foundation depth. However, the presence of sulfate minerals in the area may pose a potential risk of sulfate attack on concrete materials. Additionally, the dominant silica content in many of the rocks in the area may lead to alkali-silica reaction problems when used as construction materials. These factors should be meticulously considered in the design and construction phases of future projects to avoid potential material degradation and structural issues.

6. Conclusions and recommendations

The evaluation of foundations for the Meli gold processing plant (GPP) has determined that a suitable foundation depth is approximately 2 m below the original ground surface. However, the application of diverse empirical methodologies resulted in a wide variation in bearing capacity

estimations, ranging from 8 to 46 MPa. This highlights the novelty of our approach in utilizing multiple evaluation techniques to capture a comprehensive range of possible outcomes, enhancing the safety and reliability of foundation designs. To ensure safety, it is advisable to base the foundation design on the lowest estimated bearing capacity value. Our findings provide critical insights into assessing bearing capacity in metamorphic rock formations, thereby facilitating informed decision-making for future projects in similar geological contexts.

For future construction projects in the area, it is recommended to use standard backhoe and bulldozer trenching methods for the residual and highly weathered layers. In dry conditions, temporary slopes can be inclined at a ratio of 1 to 1 (1H:1V). Additionally, all foundations should be placed on natural ground rather than artificial-filled materials to ensure stability and minimize potential risks.

Given the presence of sulfate minerals at the site and the anticipated lifespan of future construction projects, it is crucial to select a suitable cement type, such as type-50 sulfate-resistant cement, to prevent corrosion and concrete degradation caused by chemical reactions. This proactive approach to material selection underscores the importance of considering long-term environmental factors in construction design.

Furthermore, careful layout design is advised to avoid areas with challenging ground conditions, such as the QSS unit. If avoidance is not feasible, consider placing light structures over these areas. If complete avoidance or suitable arrangements are not possible, extend the foundation depth at the QSS unit until moderately to slightly weathered rock is encountered. Additional borehole drilling is recommended for enhanced accuracy and verification, depending on the geological complexity.

In summary, for future construction projects in the area, it is advisable to consider the lowest estimated bearing capacity value for design, employ suitable construction methods and slope inclinations, ensure foundations are placed on natural ground, select corrosion-resistant cement types, make layout adjustments to avoid problematic units or ensure deeper foundation depths if necessary, and conduct additional borehole drilling for verification purposes. These measures are crucial for ensuring the safety and success of similar projects in the area.

Acknowledgments

The authors express their sincere gratitude to Ezana Mining Development PLC (EMD) for their generous financial support, which made this study possible through collaboration with Mekelle University and the provision of existing data. The authors would also like to acknowledge the invaluable support received from the staff at EMD, particularly Mr. Ataklti (CEO), Kiros Negash, Yonas Hadush, and Nebyat Adege. Their assistance and contributions have greatly contributed to the success of this research.

Use of AI tools declaration

The authors declare they have not used Artificial Intelligence (AI) tools in the creation of this article.

Data availability statement

Data cannot be made publicly available; readers should contact the corresponding authors for details.

Conflict of interest

All authors declare no conflicts of interest in this paper.

References

1. Ozsan A, Akın M (2002) Engineering geological assessment of the proposed Urus Dam, Turkey. *Eng Geol* 66: 271–281. https://doi.org/10.1016/S0013-7952(02)00047-9
2. Merifield RS, Lyamin AV, Sloan SW (2006) Limit analysis solutions for the bearing capacity of rock masses using the generalized Hoek–Brown criterion. *Int J Rock Mech Min Sci* 43: 920–937. https://doi.org/10.1016/j.ijrmms.2006.02.001
3. Kulkarni, R, Pandey VK (2021) Selection of geological parameters for design of footings on basaltic rock. *Res J Engineering Sci* 10: 43–47.
4. Bao H, Liu C, Liang N, et al. (2022) Analysis of large deformation of deep-buried brittle rock tunnel in strong tectonic active area based on macro and microcrack evolution. *Eng Failure Anal* 138: 106351. https://doi.org/10.1016/j.engfailanal.2022.106351
5. Kulhawy FH, Goodman RE (1980) Design of foundations on discontinuous rock. *Int Conf Structural Foundations Rock*, Sydney, Australia, 209–220.
6. Bastidas G, Soria O, Soria O, et al, (2022) Stability Analysis of Lava Tunnels on Santa Cruz Island (Galapagos Islands, Ecuador) Using Rock Mass Classifications: Empirical Approach and Numerical Modeling. *Geosciences* 12: 380. https://doi.org/10.3390/geosciences12100380
7. Kazmin V (1975) Explanation of the geological map of Ethiopia. Ethiopian Geological Survey Bulletin 1, Geological Survey of Ethiopia archive, 1–15.
8. Kazmin V (1978) Geology of Ethiopian basement and possible relation between the Mozambique and the Red Sea Belts. *Egypt J Geol* 22: 73–86.
9. Shackelton RM (1978) Structural development of the East African Rift System. Geological Society, London, Special Publications. 6: 19–28. https://doi.org/10.1144/GSL.SP.1978.006.01.04
10. Drury SA, Berhe SM (1993) Accretion tectonics in northern Eritrea revealed by remotely sensed imagery. *Geol Mag* 130: 177–190.
11. Tadesse T (1997) The Geology of Axum area (ND 37–6). Memoir no. 9, Ethiopian Institute of Geological Survey, Addis Ababa, Ethiopia, 184.
12. Tadesse T, Hoshino M, Sawada Y (1999) Geochemistry of low-grade metavolcanic rocks from the Pan-African of the Axum area, northern Ethiopia. *Precambrian Res* 96: 101–124. https://doi.org/10.1016/S0301-9268(99)00008-X
13. Alemu T (1998) Geochemistry of Neoproterozoic granitoids from the Axum Area, Northern Ethiopia. *J Afr Earth Sci* 27: 437–460. https://doi.org/10.1016/S0899-5362(98)00072-4

14. Ulusay R (2015) The ISRM Suggested Methods for Rock Characterization, Testing and Monitoring: 2007–2014. Pergamon Press, Oxford, UK. https://doi.org/10.1007/978-3-319-07713-0
15. International Society for Rock Mechanics (1978) Suggested methods for the quantitative description of discontinuities in rock masses. *Int J Rock Mech Min Sci Geomech Abstr* 15: 319–368. https://doi.org/10.1016/0148-9062(78)91472-9
16. Rockware (2010) *Rockworks15 Manual*, 3rd Ed., Rockware, Inc. USA.
17. Bieniawski ZT (1989) *Engineering rock mass classifications: a complete manual for engineers and geologists in mining, civil, and petroleum engineering*, Wiley, New York, 251.
18. Barton N, Lien R, Lunde J (1974) Engineering classification of rock masses for the design of tunnel support. *Rock Mech* 6: 189–236. https://doi.org/10.1007/BF01239496
19. Hoek E, Brown ET (1997) Practical estimates of rock mass strength. *Int J Rock Mech Min Sci* 34: 1165–1186. https://doi.org/10.1016/S1365-1609(97)80069-X
20. Fookes PG, Sweeney M, Manby CND, et al. (1985) Geological and geotechnical engineering aspects of low-cost roads in mountainous terrain. *Eng Geol* 21: 1–152. https://doi.org/10.1016/0013-7952(85)90002-X
21. Kulhawy FH, Carter JP (1992) Settlement and bearing capacity of foundations on rock masses and socketed foundations in rock masses. *Engineering in rock masses*, Butterworth-Heinemann, Oxford, 231–245.
22. Goodman RE (1991) *Introduction to Rock Mechanics*, 2nd Ed., Wiley, New York, 562.
23. Serrano A, Olalla C, Gonzalez J (2000) Ultimate bearing capacity of rock masses based on the modified Hoek-Brown criterion. *Int J Rock Mech Min Sci* 37: 1013–1018. https://doi.org/10.1016/S1365-1609(00)00028-9
24. USACE (1994) Rock Foundations. Department of the Army U.S. Army Corps of Engineers Washington, DC. Available from: https://www.scribd.com/document/577794118/rock-foundations-em-111012908
25. Ezana Mining Development PLC (2010) Geological report on Meli Gold Project (Technical Report), Mekelle, Ezana Mining Development PLC (Ethiopia) archive. Ethiopia.
26. Berhane G, Kidanu S, Abera T (2011) Engineering geological study report on Meli Gold project, northwestern zone of Tigray, Ethiopia (Technical Report). Ezana Mining Development PLC, Mekelle, Ezana Mining Development PLC (Ethiopia) archive. Ethiopia.
27. Jembere D, Yihdego Y (2016) Engineering Rock Mass Evaluation for a Multi-purpose Hydroelectric Power Plant: Case of Genale Dawa (GD-3), Ethiopia. *Geotech Geol Eng* 34: 1593–1612. https://doi.org/10.1007/s10706-016-0068-9
28. Hoek E, Kaiser PK, Bawden WF (2000) *Support of underground excavations in hard rock*. CRC Press, 215.
29. Grimstad E, Barton N (1993) Updating the Q-System for NMT. Proc Int Symp on Sprayed Concrete-Modern Use of Wet Mix Sprayed Concrete for Underground Support, Fagernes, Oslo: Norwegian Concrete Assn. Available from: https://www.researchgate.net/publication/312619292_Updating_the_Q-system_for_NMT
30. Marinos P, Hoek E (2001) Estimating the geotechnical properties of heterogeneous rock masses such as flysch. *Bull Eng Geol Environ* 60: 85–92. https://doi.org/10.1007/s100640000090
31. Hoek E, Carranza-Torres C, Corkum B (2002) Hoek-Brown failure criterion-2002 edition. *Proc NARMS-Tac Conf* 1: 267–273.

32. Rocscience (2007) RocLab software manual. Rocscience Inc., Canada. Available from: https://www.resolutionmineeis.us/documents/rocscience-2007
33. Ozsan A, Karpuz C (1996) Geotechnical rock-mass evaluation of the Anamur dam site, Turkey. *Eng Geol* 42: 65–70. https://doi.org/10.1016/0013-7952(95)00065-8
34. Serrano A, Olalla C (1994) Ultimate bearing capacity of rock masses. *Int J Rock Mech Min Sci Geomech Abstr* 31: 93–106. https://doi.org/10.1016/0148-9062(94)92799-5

AIMS Press